Journal of Magnetism and Magnetic Materials 480 (2019) 101–107

Contents lists available at ScienceDirect

Journal of Magnetism and Magnetic Materials

journal homepage: www.elsevier.com/locate/jmmm

Research articles

Noncollinear magnetism in Lithium-doped zigzag graphene nanoribbons

J.T. Liang[a], X.H. Yan[a,b,c,*], Y. Zhang[a,*], Y.D. Guo[c], Y. Xiao[a,*]

[a] College of Science, Nanjing University of Aeronautics and Astronautics, Nanjing 210016, China
[b] School of Material Science and Engineering, Jiangsu University, Zhenjiang 212013, China
[c] Key Laboratory of Radio Frequency and Micro-Nano Electronics of Jiangsu Province, Nanjing University of Posts and Telecommunications, Nanjing 210023, China

A B S T R A C T

Based on density functional theory and non-equilibrium Green's function method, we studied noncollinear magnetism and electronic transport in zigzag graphene nanoribbon (ZGNR) doped with Li atom. Compared to pristine ZGNR, the Li-doped ZGNR presents characteristic features of magnetization distribution, which depends on the position of Li atom. When the magnetizations of two leads are parallel, i.e. $\theta = 0°$, the Li atom induces an antiferromagnetic order on the edge, which is attributed to the change in exchange strength due to charge transfer. As for nonzero θ, the magnetization distribution in the case of interior adsorption shows obvious spin spiral. However, in edge adsorption, the spin spiral does not occur and a two-region feature appears. Moreover, the rotation sense of magnetization for edge adsorption becomes counter-clockwise which is different from the interior adsorption. The transmission presents distinct features for edge and interior adsorption. As $\theta = 180°$, the transmission coefficient at Fermi level is about two for interior adsorption but drops to about one in edge adsorption. These results provide considerable insights into the effect of doping on noncollinear magnetism and spin transport in ZGNR.

1. Introduction

Owing to its two-dimensional (2D) atomic structure, graphene has become a hot topic in both theoretical physics, material science and application sciences [1–5]. The graphene also boosts the development of 2D materials, e.g. transition metal dichalcogenide [6,7]. Various physics and devices in electronic, magnetic, optical fields are proposed and realized [8–10]. Among them, spintronic properties and application are especially promising due to the design of carbon-based devices and the search for magnetism in non-magnetic materials. Currently, it is well-known that cutting the graphene to have a zigzag edge will bring an asymmetry in the A(B) sublattice and therefore reproduce magnetism in graphene [11]. A number of studies have been devoted to zigzag graphene nanoribbon (ZGNR) in order to reveal characteristic spintronic feature and make spintronic devices [12,13]. Tombros et al. have performed electronic transport measurement and found that spin can travel for a long distance in graphene [14]. This experimental result implies that graphene may be a good candidate for spintronic applications. To this end, several theoretician studied the possibility of designing ZGNR-based nanoelectronic devices by calculating the transmission and current-voltage curve. Many interesting features, such as the dependence of transmission and current on structural symmetry, spin polarity, and bias voltage, are revealed [15–20]. These studies provide considerable insights into the understanding of spintronic properties and applications of ZGNR.

Current theoretical and experimental studies of ZGNR are mostly concentrated on the collinear magnetism. This is physically appropriate because noncollinear magnetic order is energetically unfavorable in a pure and undoped ZGNR. As is known, the noncollinear magnetism usually takes place in a system with strong spin-orbit coupling or competition of exchange interaction [21–23]. But, the spin-orbit interaction in graphene has been proved to be small [24]. On the other hand, the ZGNR is of small magnetic moment ($0.25\mu_B$ per atom) and therefore the exchange interaction between the first nearest neighbors dominates over the second one [25]. In order to realize noncollinear magnetism in ZGNR, it is necessary to introduce perturbation into graphene lattice such as doping, adsorption or other means. Yazyev and Katsnelson studied the exchange stiffness of a spin spiral in ZGNR and considered the effect of defect on the edge on noncollinear magnetism [26]. Moreover, Zhang et al. considered a different method by building a two-probe model based on ZGNR and introducing the noncollinear magnetization in left and right leads [27]. Under the constraint of lead magnetizations, the central region displays pronounced spin spiral, which depends on the length of central region and the twist angle between left and right lead magnetizations. Some interesting feature in transport properties, e.g. the insensitivity of transmission coefficient at the Fermi level with respect to the noncollinear magnetism, are revealed.

Although Ref. [27] has presented many details on noncollinear magnetism, the model used there is far too ideal to be used to design a realistic device. In an experiment, the defect, dopant and adsorbate remain more or less in the sample. Therefore, it is natural to ask: What

* Corresponding authors.
E-mail addresses: xhyan@nuaa.edu.cn (X.H. Yan), yingzhang@nuaa.edu.cn (Y. Zhang), yxiao263@gmail.com (Y. Xiao).

https://doi.org/10.1016/j.jmmm.2019.02.072
Received 9 October 2018; Received in revised form 31 January 2019; Accepted 22 February 2019
Available online 23 February 2019
0304-8853/ © 2019 Published by Elsevier B.V.

is the noncollinear magnetization distribution in a doped ZGNR? How does the dopant affect the noncollinear transmission? To answer this question, we extend the calculation in Ref. [27] to the case with the lithium dopant. We focus on the effect of Li doping on noncollinear magnetism and transmission coefficient. Several new results and physics are discussed and revealed.

The remainder of the paper is organized as follows. In Sec. II, we show the computational method and structural model of Li-doped ZGNR. The construction of initial magnetization distributions of spin-spiral are discussed. In Sec. III, the results of magnetization distribution and transmission coefficient are given. The physical mechanisms are discussed. The findings are concluded in Sec. IV.

2. Computational methods and models

The calculation is performed in a two-probe geometry which consists of left, right leads and the central region. Since electronic structure of two leads keeps fixed in the self-consistent process, we are treating a problem of fixed boundary condition. This is different from traditional first-principle calculations with periodic boundary condition. For this kind of problems, we employ the density functional theory (DFT) combined with non-equilibrium Green's function method (NEGF) [28–32] as implemented in OpenMX package [33]. Firstly, the Hamiltonian of both central region and leads are constructed in the local density approximation (LDA) of DFT with norm-conserving pseudopotentials. Different from the plane-wave calculation, the pseudoatomic orbitals (PAOs) are used in order to expand the wave function. The PAOs for carbon, lithium and hydrogen atoms are C5.0-s2p1, Li7.0-s2p2 and H5.0-s2p1 where 5.0 and s2p1 represent the cutoff radius (in Bohr unit) of atomic orbital and the number of primitive atomic orbitals used. The energy cutoff for real space integration and the solution of Poisson equation is 300 Ry. Secondly, the Green's function is calculated using the Hamiltonian of central region and the self-energies of both leads. Then, the density matrix is directly evaluated with the Green's function. The charge density, which is an important quantity in DFT, is calculated from the density matrix and iterated until the convergence is reached. The electronic temperature is 300 K in all calculations. In noncollinear magnetism, we usually choose two types of spin quantization axis [34,35], i.e. global and local axis. The global axis is always along the z axis. The local axis is along the direction of each atom's magnetization, which varies from atom to atom. After the convergence is achieved, the transmission coefficient is calculated by the converged Green's function and the Landauer formula.

The device geometry is shown in Fig. 1. The ZGNR under consideration is mirror symmetric with respect to the midplane between two edges. The sublattice along the z direction contains eight carbon atoms. Along the transport direction (y), the length of central region equals $L_y = (N_{edge} - 1)a$ with $a = \sqrt{3}\,a_{c-c}$ where a_{c-c} is the distance between two neighbouring carbon atoms. N_{edge} is the number of carbon atom in the edges. In this work, we consider $N_{edge} = 17$. A spiral-like magnetization distribution is selected as the initial condition for self-consistent calculation. The local magnetic moment of carbon atom on the edge along the ZGNR rotates between two lead magnetizations in constant step of $\frac{180^\circ}{N_{edge}-1}$. Moreover, we also consider another initial condition in order to study the effect of initial condition on magnetization distribution. In order to obtain convergence, a certain of buffer layers are added into the left and the right sides of central region. One Li atom is located above the center of the hexagon of graphene lattice, which is the stablest position for most alkali metals. The height of Li atom on the graphene (1.78Å) is fully relaxed prior to DFT/NEGF calculations. We consider two types of Li adsorption, i.e. Li atom at the edge and in the interior of ZGNR, which is denoted by the number 1 and 2 in Fig. 1.

The noncollinear magnetism is implemented by setting the magnetization of left lead along the z axis while that of right lead canted with an angle θ. Prior to DFT/NEGF calculations, the electronic structure with noncollinear magnetization in left and right leads are obtained by traditional DFT calculations. Then, electronic structure of the central region is obtained by virtue of self-consistent iteration under the constraint of lead magnetizations. The amplitude and direction of magnetic moments of all atoms in central region are fully relaxed.

3. Results and discussions

We first show the magnetization and transmission coefficient of undoped ZGNR with $\theta = 0°$ and $\theta = 180°$ as shown in Fig. 2. As $\theta = 0°$, one can see a ferromagnetic order on both top and bottom edges of ZGNR. This is reasonable since the uniform magnetization of left and right leads (along the z axis) will force the magnetization of central region to align with lead magnetization. The ferromagnetic order presented here is different from those found in previous studies [11]. It is found from both tight-binding [11] and DFT [36] calculations that the antiferromagnetic coupling between magnetizations of top and bottom zigzag edges is energetically stabler than the ferromagnetic coupling for ZGNR. To verify this, we also performed traditional DFT calculations, instead of DFT/NEGF calculations. In the DFT calculations, the unit cell consists of 32 carbon atoms and 4 hydrogen atoms and the lattice constant along the y axis is $2a$. The calculation shows that the total energy of antiferromagnetic coupling is about 8 meV smaller than that of ferromagnetic coupling. However, in realistic device, there will be direct coupling between ZGNR and leads, which may suppress the antiferromagnetic coupling between upper and bottom edges. Therefore,

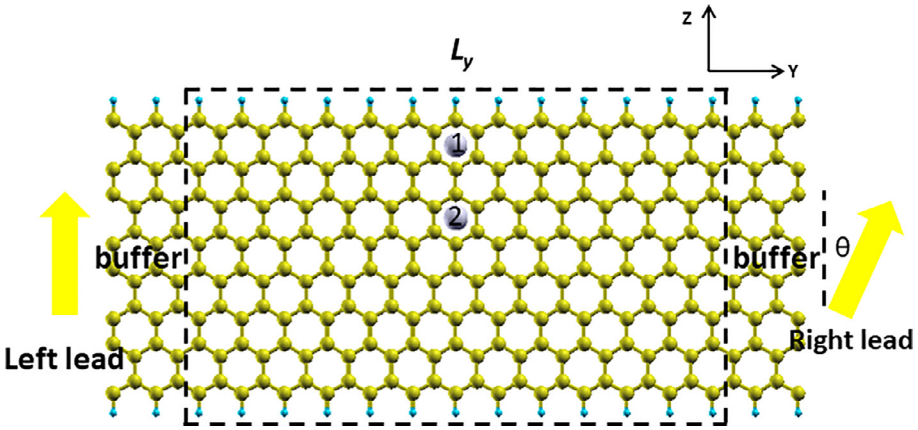

Fig. 1. Structural model of two-probe device under consideration. It consists of left lead, central region and right lead. In the central region, two buffer regions are used in our calculations. The magnetization of left lead (left thick arrow) makes an angle θ with the magnetization of the right lead (right thick arrow). The dangling bonds on the edge atoms are saturated by hydrogen atoms. The numbers 1 and 2 indicate the position of Li atom for edge and interior adsorption.

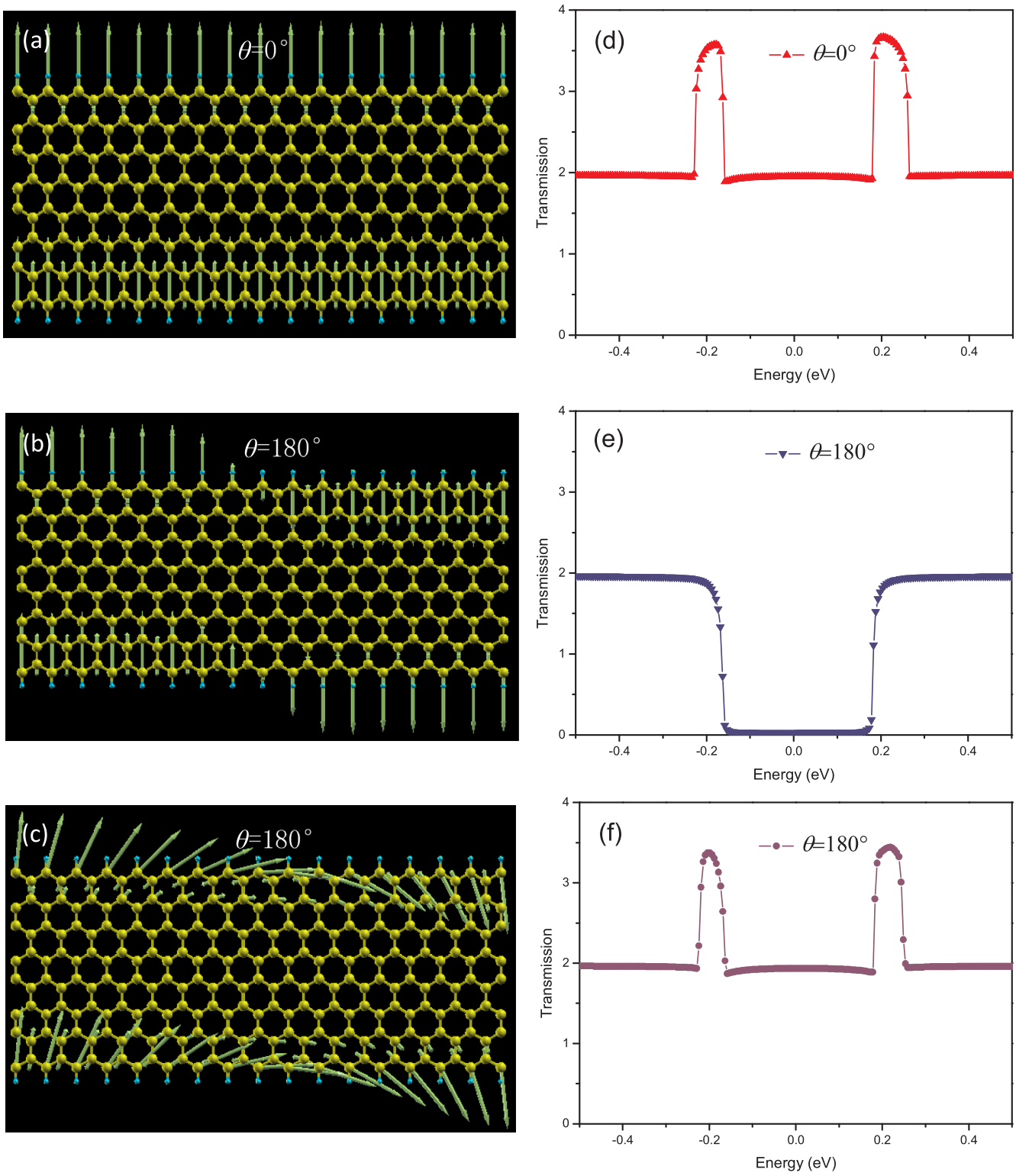

Fig. 2. Magnetization distribution of undoped ZGNR for (a) $\theta = 0°$, (b) $\theta = 180°$ with collinear magnetism and (c) $\theta = 180°$ with spin spiral. (d)~(f) are the same as (a)~(c) but for transmission coefficient.

we still consider the ferromagnetic order between upper and bottom edges in our calculations. As $\theta = 180°$, the relaxed magnetization distribution depends on the initial condition. If the initial condition is collinear (Fig. 2(b)), the relaxed magnetic profile shows an abrupt domain wall. But for the spiral initial condition (Fig. 2(c)), a spiral domain wall is favorable. This phenomenon has been found in atomic chain of transition metal elements [37–42].

Moreover, we calculate the total energy of two magnetization distributions shown in Fig. 2 (b) and (c) based on the traditional DFT method. Since the 180° domain wall does not satisfy periodic boundary condition, we consider the unit cell with twice the length shown in Fig. 2. That is to say, it is (↑)-(↓)-(↑) for Fig. 2 (b) while (↑)-(spiral)-(↓)-(spiral)-(↑) for Fig. 2(c). For the spiral domain wall, a constrained scheme with the added penalty functional [28] is employed in the self-

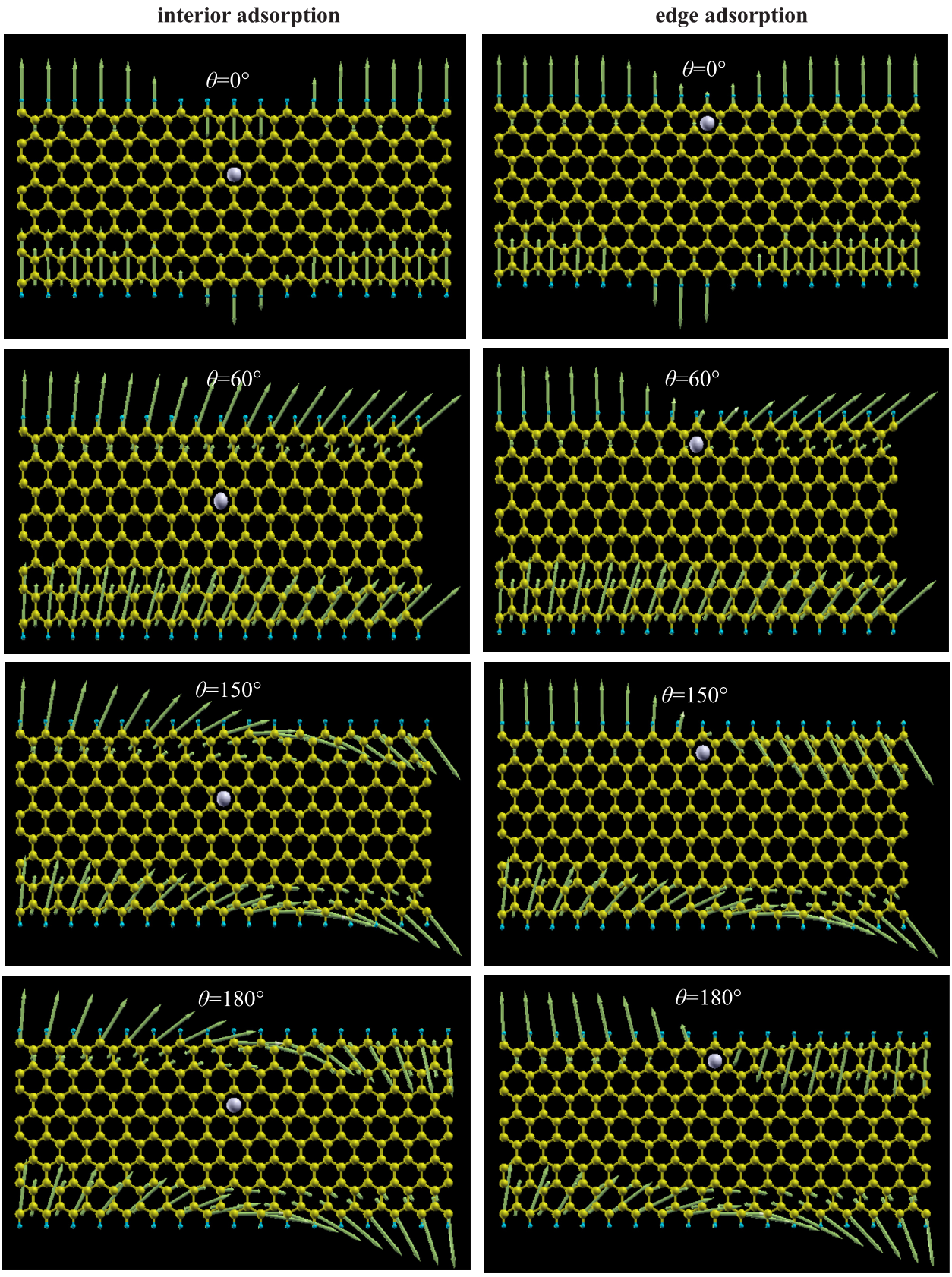

Fig. 3. Magnetization distribution of Li-doped ZGNR for interior and edge adsorption at various θ. In the self-consistent calculations, the initial magnetization is taken to be spiral distribution.

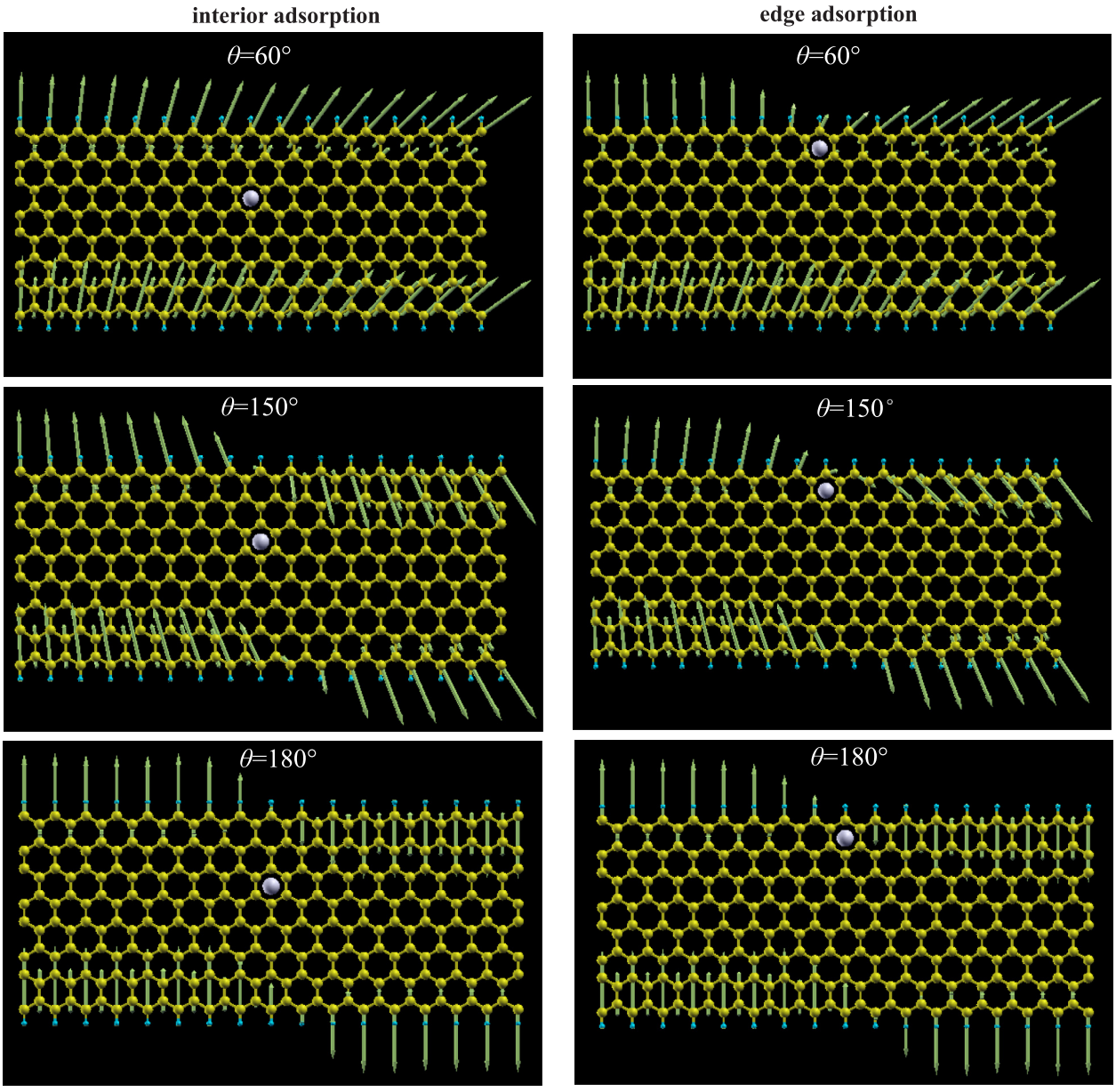

Fig. 4. The same as Fig. 3 but the initial magnetization is taken to be lead-like distribution.

consistent calculations. The result shows that the total energy of spiral domain wall is about 150 meV smaller than that of the abrupt domain wall. This energetic stability can be understood from the Heisenberg exchange interaction between two neighboring magnetizations $\vec{M}_i$ and $\vec{M}_j$, *i. e.* $H = -J\vec{M}_i \cdot \vec{M}_j$ with J the exchange integral. As for the abrupt domain wall, the 180° spin flip promotes the total energy greatly. But for spiral domain wall, the angle between two neighboring magnetizations is small and thus the increase in total energy is small as well. From an energetic point of view, the spiral magnetization distribution is more favorable than the collinear one.

The transmission coefficient at $\theta = 0°$ as shown in Fig. 2 (d) is either two or four depending on the electronic energy. This could be understood by the fact that, in a undoped and periodic system, the transmission at an arbitrary energy will be determined by the number of electronic states. Near the Fermi level, a ZGNR has two or four electronic states which has been verified in a number of literatures [11,27]. As $\theta = 180°$, the transmission of abrupt domain wall is much lower than that of spiral one. As seen in Fig. 2 (b), there is an abrupt change of spin direction in the middle of central region. This abrupt change brings a strong spin-flip scattering and therefore hinders the spin transport along the ZGNR. However, in the spiral domain wall, the transmission is enhanced by the spin mixing effect, for which two independent spin channels (up-spin and down-spin) in collinear magnetism are hybridized in noncollinear magnetism [37]. In such case, we can not refer to up-spin and down-spin since these two spin channels are no longer recognized. Due to spin mixing effect, some transmission channels, which is forbidden in collinear magnetism, will be made possible and thus the transmission is greatly enhanced. Moreover, the smaller the relative angle θ is, the weaker the spin flip scattering is and the higher the transmission is. This is the reason why only a little difference between transmissions at $\theta = 0°$ and $\theta = 180°$ (helical) exists.

Next we show the results of Li-doped ZGNR in Fig. 3. As the Li atom resides in the interior of ZGNR (left panel of Fig. 3), the magnetization distribution is quite different from that of undoped ZGNR. At $\theta = 0°$, one can clearly see two changes which are induced by the dopant. First, the magnetic moment near the dopant is suppressed. This makes the size of magnetic moment decreases from the carbon atoms near the leads to the dopant region. This suppression in magnetic moment is due

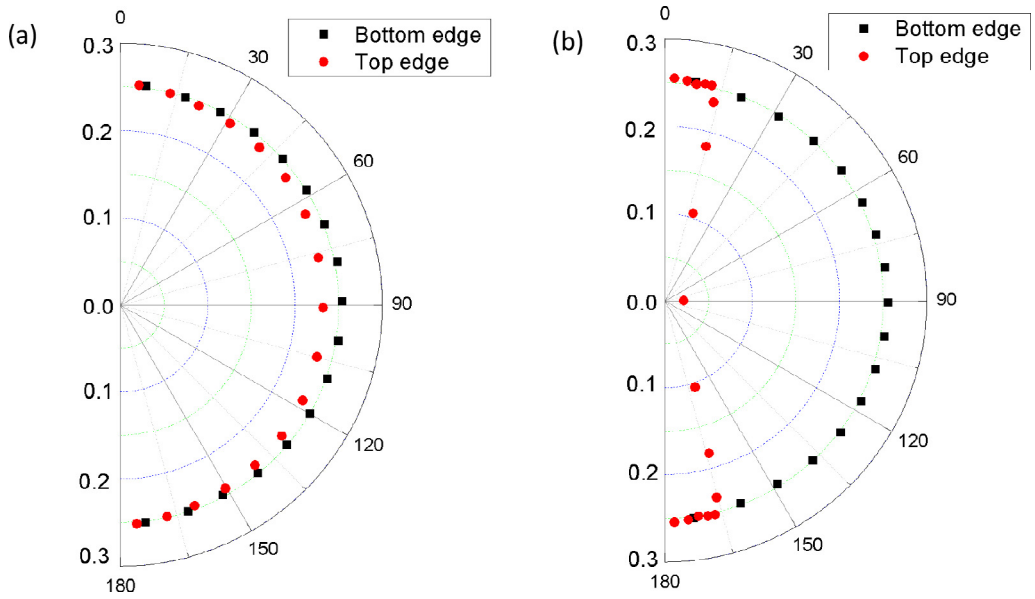

Fig. 5. Polar plot of the direction and size of local magnetic moments along the transport direction at $\theta = 180°$ for (a) interior and (b) edge adsorption. The magnetic moments of carbon atoms on the top and bottom edges are shown. Each point (circles and squares) corresponds to an carbon atom on the edge. The size of magnetic moment is represented by the length from the sphere to the center of circle. The unit of magnetic moment is μ_B. The direction of magnetic moment is represented by the azimuth from the vertical line to the sphere in the polar plot.

to the orbital hybridization between the carbon atoms and the Li atom, which has been found in magnetic material doped by carbon or boron atoms [43]. Second, an antiferromagnetic order occurs in each edge. This could be explained by charge transfer, which changes the exchange strength in ZGNR. Our calculation predicts that the negative charge is transferred from the Li atom to the surrounding carbon atoms. Such charge transfer changes the bonding between carbon and carbon atoms, thereby influences the exchange interaction as well. Since charge transfer is a local effect, the magnetization far away from the dopant remains unchanged.

However, the above two phenomena do not appear any more as $\theta \neq 0°$ for interior adsorption. At $\theta = 60°$, 150° and 180°, one can see that the magnetization of each edge follows a spiral-like distribution. There are no magnetization suppression and no antiferromagnetic order at the edge. This behavior is analogous to those found in undoped ZGNR shown in Fig. 2. This could be attributed to strong exchange interaction arising from left and right leads. As magnetizations of two leads are made by θ, the carbon atoms near the left (right) lead will align their magnetization with that of left (right) lead due to the exchange interaction. Although the Li atom will alter the exchange interaction near the Li atom, the exchange interaction in the noncollinear case is strong enough to dominate over the influence of Li atom in the case of interior adsorption. Therefore, a spin spiral exists even in the presence of Li doping.

As the Li atom is located at the edge, i.e. the edge adsorption, the change induced by the Li atom becomes more pronounced compared to the interior adsorption. At $\theta = 0°$, the magnetization of in the middle of top edge is suppressed. The antiferromagnetic order occurs in the bottom edge instead of the top edge. This indicates that a stronger coupling between carbon and Li atom is built in the edge adsorption than in the interior adsorption. As $\theta \neq 0°$, several interesting behavior can be seen. The top edge and bottom edge present quite different features. In the bottom edge, the spin spiral still exists. But in the top edge, no spin spiral is present. In contrary, the top edge can be divided into two parts, i.e. left and right regions. In the left (right) regions, the magnetizations of edge atoms resemble like those in left (right) leads. Such a two-region feature will be useful since it provides us with a new means to tuning the magnetization of ZGNR. Moreover, the rotation sense of magnetization in the top edge alters, which is especially obvious at large θ. For interior adsorption, the magnetization in the top edge rotates clockwise from left to right in central region. But for edge adsorption, as seen at $\theta = 180°$, the rotation sense of magnetization becomes counter-clockwise. The change in rotation sense usually takes place in magnetic material with large spin-orbit interaction [21–23]. The results of ZGNR reported here may be important for understanding magnetic interaction in carbon system.

Despite the intriguing magnetization distribution found in Fig. 3, it should be emphasized that the resulting magnetization distribution is actually determined by the initial condition of magnetization. To demonstrate it, we consider another initial condition in self-consistent calculation. The initial condition in Fig. 3 is the spiral magnetization distribution as detailed in Sec. II. The second initial condition is called the lead-like magnetization distribution. In this initial condition, the ZGNR is divided into left and right parts which occupy one half of the ribbon respectively. The magnetization of each edge atom in left (right) part is set to be parallel to the left (right) lead magnetization. Once the initial condition is set, the self-consistent convergence will give rise to the relaxed magnetization distribution shown in Fig. 4. One can see that the magnetization near the dopant is suppressed while those magnetization far away from the dopant follows the lead magnetization for both upper and bottom edges. The comparison between Fig. 3 and Fig. 4 indicates that the initial condition is important in determining the magnetization distribution of Li-doped ZGNR.

To be more illustrative, we show the variation in the amplitude and direction of magnetization at $\theta = 180°$ in Fig. 5. In the case of edge adsorption, the bottom edge shows a spin spiral with the size of magnetization almost unchanged ($0.25\mu_B$). The top edge presents a two-region feature with the exception of a few edge atoms in the middle. As for the interior adsorption, both top and bottom edges give rise to spin spiral, which implies that the interior adsorption of Li atoms has small influence on magnetization distribution.

Finally, we discuss spin transport in Li-doped ZGNR for both types of adsorption. As shown in Fig. 6(a), the interior adsorption at $\theta = 0°$ displays almost the lowest transmission. Compared to other angles, the transmission at $\theta = 0°$ drops greatly and there is a dip with zero transmission near the Fermi level. This dip indicates the formation of the quasi-bound state [44], which is arisen from the backscattering in the case of Li doping. As mentioned previously, the spin-flip scattering

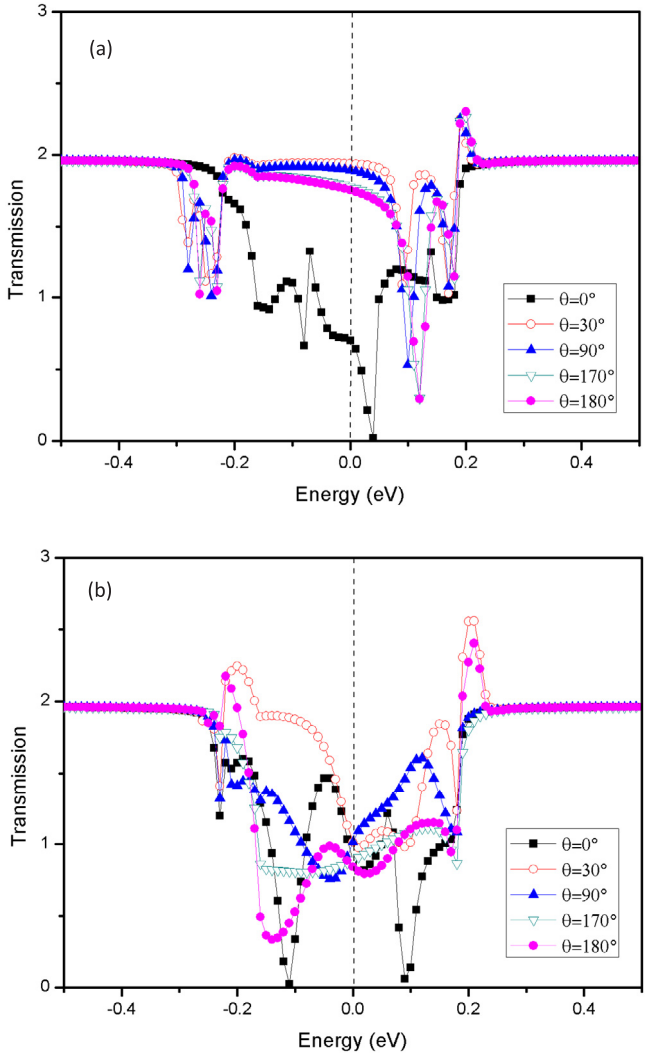

Fig. 6. Transmission as function of energy for (a) interior and (b) edge adsorption at several θ.

does not play a role near the Fermi level. For all nonzero θ, the transmission at the Fermi level is nearly equal to two. So, the impurity scattering dominates at $\theta = 0°$ while the spin-flip scattering comes into play as θ becomes finite. Compared to the interior adsorption, the edge adsorption presents similar behavior shown in Fig. 6(b). The electron transmission is suppressed due to backscattering. But, the difference lies mainly in the position of quasibound state. At $\theta = 0°$, there are two symmetric dips near the Fermi level. At $\theta = 180°$, there is a dip just near the Fermi level, which is absent in the interior adsorption. This could be used for the design of the ZGNR-based devices in future experiments. For example, the transmission of interior adsorption is about two at the Fermi level, while it decreases to one for edge adsorption. Therefore, these two cases can be used to design the "On" and "Off" states, which may be useful for potential applications in nanoelectronic devices.

4. Conclusion

In summary, we calculated magnetization distribution and transmission coefficient of Li-doped ZGNR based on first-principle calculations. The results show that the magnetization distribution is much different from undoped ZGNR. The magnetic moment of edge carbon atom rotates itself like a spin spiral in the undoped ZGNR. However, the magnetization distribution of doped ZGNR depends on the location of Li atom. As for the interior adsorption, the spin spiral exists in both top and bottom edges. But for edge adsorption, the spin spiral occurs only in the edge without the Li doping. In the edge with Li atom, a two-region feature appears. The magnetic moments of left (right) side of central region follow those of left (right) lead. Another interesting point is that the clockwise rotation sense of magnetization for interior adsorption changes to counter-clockwise one. Moreover, as $\theta = 0°$, the magnetic order becomes antiferromagnetic on an edge due to the change in exchange strength induced by charge transfer. The transmission presents many characteristic features, which reveals the combined effect of impurity scattering and spin flip scattering. As $\theta = 180°$, the transmission coefficient at Fermi level is about two in interior adsorption but drops to about one. We believe the results reported in this paper could be of potential interest in future studies of ZGNR-based nanoelectronic devices.

Acknowledgements. This work is supported by the National Natural Science Foundation of China (NSFC11804158, NSFC91750112 and NSFC11504178). YX. would like to thank Prof. Taisuke Ozaki for his generous hospitality when visiting his group at JAIST.

References

[1] A.K. Geim, K.S. Novoselov, Nat. Mat. 6 (2007) 183.
[2] A.H. Casto Neto, F. Guinea, N. Peres, Rev. Mod. Phys. 81 (2013) 109.
[3] J. Zhou, T. Hu, J.M. Dong, Y. Kawazoe, Phys. Rev. B 86 (2012) 035434.
[4] P. Cui, Q. Zhang, H.B. Zhu, X.X. Li, W.Y. Wang, Q.X. Li, C.G. Zen, Z.Y. Zhang, Phys. Rev. Lett. 116 (2016) 026802.
[5] A. Pachoud, A. Ferreira, B. Ozyilmaz, A.H. Castro Neto, Phys. Rev. B 90 (2014) 035444.
[6] D. Xiao, G. Liu, W. Feng, X. Xu, W. Yao, Phys. Rev. Lett. 108 (2012) 196802.
[7] W. Feng, Y. Yao, W. Zhu, J. Zhou, W. Yao, D. Xiao, Phys. Rev. B 86 (2012) 165108.
[8] B. Huang, F. Liu, J. Wu, B.L. Gu, W. Duan, Phys. Rev. B 77 (2008) 153411.
[9] M. Gmitra, J. Fabian, Phys. Rev. B 92 (2015) 155403.
[10] W. Zhang, F. Hajiheidari, R. Mazzarello, Phys. Rev. B 96 (2017) 245413.
[11] M. Fujita, K. Wakabayashi, K. Nakada, K. Kusakabe, J. Phys. Soc. Jpn. 65 (1996) 1920.
[12] Z. Bai, L. Shen, Y. Cai, Q. Wu, M. Zeng, G. Han, Y.P. Feng, New J. Phys. 16 (2014) 103033.
[13] J. Lee, J. Fabian, Phys. Rev. B 94 (2016) 195401.
[14] N. Tombros, C. Jozsa, M. Popinciuc, H.T. Jonkman, B.J. van Wees, Nature 448 (2007) 571.
[15] S. Okada, A. Oshiyama, Phys. Rev. Lett. 87 (2001) 146803.
[16] K. Sawada, F. Ishi, M. Saito, S. Okada, T. Kawai, Nano Lett. 9 (2009) 269.
[17] Z. Li, H. Qian, J. Wu, W.H. Duan, Phys. Rev. Lett. 100 (2008) 206802.
[18] J. Jung, T. Pereg-Barnea, A.H. MacDonald, Phys. Rev. Lett. 102 (2009) 227205.
[19] J.E. Padilha, R.B. Pontes, A.J.R. da Silva, Solid State Commun. 173 (2013) 24.
[20] V. Meunier, A.G. Souza Filho, E.B. Barros, Rev. Mod. Phys. 88 (2016) 025005.
[21] T. Oda, A. Pasquarello, R. Car, Phys. Rev. Lett. 80 (1998) 3622.
[22] R. Wiesendanger, Rev. Mod. Phys. 81 (2009) 1495.
[23] M. Bode, M. Heide, K. von Bergmann, P. Ferriani, S. Heinze, S. Blugel, R. Wiesendanger, Nature 447 (2007) 190.
[24] Y. Yao, F. Ye, X.L. Qi, S.C. Zhang, Z. Fang, Phys. Rev. B 75 (2007) 041401(R).
[25] T. Ozaki, K. Nishio, H. Weng, H. Kino, Phys. Rev. B 81 (2010) 075422.
[26] O. Yazyev, M.I. Katsnelson, Phys. Rev. Lett. 100 (2008) 047209.
[27] Y. Zhang, X.H. Yan, Y.D. Guo, Y. Xiao, J. Appl. Phys. 121 (2017) 174303.
[28] T. Ozaki, H. Kino, Phys. Rev. B 72 (2005) 045121.
[29] J.M. Soler, E. Artacho, J.D. Gale, A. Garcia, J. Junquera, P. Ordejon, D. Sanchez-Portal, J. Phys.: Condens. Matter 14 (2002) 2745.
[30] J. Taylor, H. Guo, J. Wang, Phys. Rev. B 63 (2001) 121104.
[31] I. Rungger, S. Sanvito, Phys. Rev. B. 78 (2008) 035407.
[32] M. Brandbyge, J. Mozos, P. Ordej'n, J. Taylor, K. Stokbro, Phys. Rev. B 65 (2002) 165401.
[33] Seehttp://www.openmx-square.org/ for the details of DFT/NEGF method as implemented in OpenMX.
[34] I. Zutic, J. Fabian, S. Das Sarma, Rev. Mod. Phys. 76 (2004) 323.
[35] J. Kubler, K.H. Hock, J. Sticht, J. Phys. F 18 (1988) 469.
[36] Y. Zhang, X.H. Yan, Y.D. Guo, Y. Xiao, Phys. Lett. A 381 (2017) 2949.
[37] J.D. Burton, R.F. Sabirianov, S.S. Jaswal, E.Y. Tsymbal, Phys. Rev. Lett. 97 (2006) 077204.
[38] N. Garcia, M. Munoz, Y.W. Zhao, Phys. Rev. Lett. 82 (1999) 2923.
[39] M.R. Sullivan, D.A. Boehm, D.A. Ateya, S.Z. Hua, H.D. Chopra, Phys. Rev. B 71 (2005) 024412.
[40] H.D. Chopra, M.R. Sullivan, J.N. Armstrong, S.Z. Hua, Nat. Mater. 4 (2005) 832.
[41] M. Czerner, B.Yu. Yavorsky, I. Mertig, J. Appl. Phys. 103 (2008) 07F304.
[42] M. Czerner, B.Yu. Yavorsky, I. Mertig, Phys. Status Solidi B 247 (2010) 2594.
[43] M.R. Press, F. Liu, S.N. Khanna, P. Jena, Phys. Rev. B 40 (1989) 399.
[44] B. Biel, X. Blase, F. Triozon, S. Roche, Phys. Rev. Lett. 102 (2009) 096803.